
SHTOcc: Effective 3D Occupancy Prediction with Sparse Head and Tail Voxels

Qiucheng Yu

City University of Hong Kong

qiuchenyu2-c@my.cityu.edu.hk

Yuan Xie

East China Normal University

yxie@cs.ecnu.edu.cn

Xin Tan*

East China Normal University

xtan@cs.ecnu.edu.cn

Abstract

3D occupancy prediction has attracted much attention in the field of autonomous driving due to its powerful geometric perception and object recognition capabilities. However, existing methods have not explored the most essential distribution patterns of voxels, resulting in unsatisfactory results. This paper first explores the inter-class distribution and geometric distribution of voxels, thereby solving the long-tail problem caused by the inter-class distribution and the poor performance caused by the geometric distribution. Specifically, this paper proposes SHTOcc (Sparse Head-Tail Occupancy), which uses sparse head-tail voxel construction to accurately identify and balance key voxels in the head and tail classes, while using decoupled learning to reduce the model’s bias towards the dominant (head) category and enhance the focus on the tail class. Experiments show that significant improvements have been made on multiple baselines: SHTOcc reduces GPU memory usage by 42.2%, increases inference speed by 58.6%, and improves accuracy by about 7%, verifying its effectiveness and efficiency. The code is available at <https://github.com/ge95net/SHTOcc>.

1 Introduction

Vision-based 3D occupancy prediction (3D Occ) constitutes a fundamental task in 3D scene understanding, requiring simultaneous estimation of occupancy states and semantic labels for each voxel within a volumetric space. This capability forms a critical component for robotic navigation and autonomous driving systems [1, 2, 3], necessitating the development of computationally efficient feature processing methods to ensure reliable predictions. The inherent structural regularity of 3D voxel distributions provides valuable prior knowledge that remains underutilized in current approaches.

Contemporary methods fall into two primary categories: (1) *Distribution-independent methods* approaches, including image-based implementations [4, 5, 6, 7, 8, 9, 10] and video-based extensions [11, 12, 13], process complete 3D volumes through specialized decoders for per-voxel classification. (2) *Partial Distribution-Aware Methods* techniques such as TPV [14, 15, 16], 3D Gaussian Splatting (3DGS) [17, 18, 19], and SparseOcc [20, 21, 22, 23] exploit voxel sparsity by focusing computations on occupied regions. While these methods demonstrate progressive improvements, they inadequately exploit two fundamental distribution patterns: (a) inter-class distribution and (b) geometric distribution. Our work systematically addresses both aspects through explicit distribution-aware modeling.

*Corresponding author

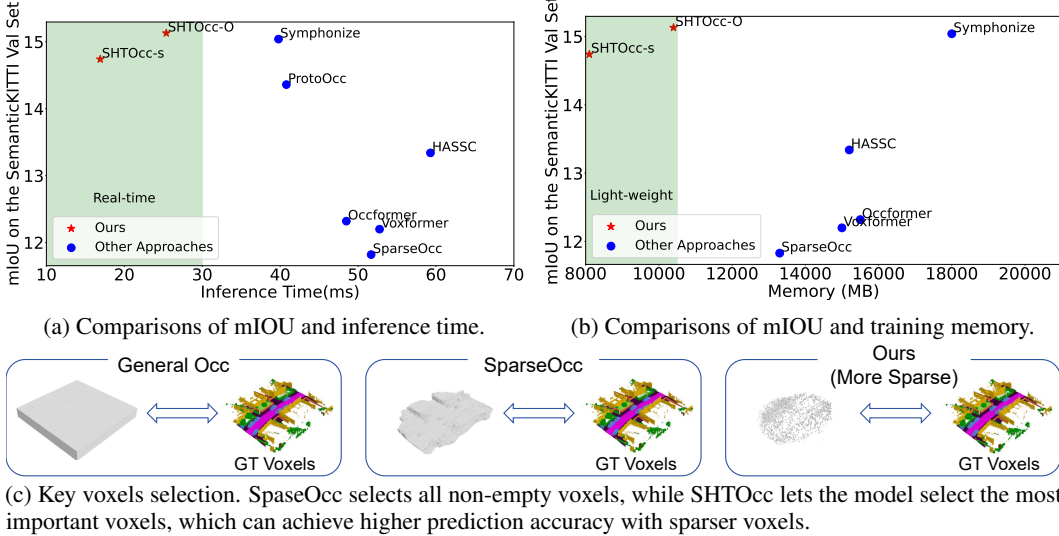


Figure 1: Comparisons of the SHTOCC of various 3D semantic scene completion methods on the SemanticKITTI [1] dataset.

The inter-class distribution of voxels describes the varying frequency distribution across different object classes. We observe a pronounced long-tail distribution problem in 3D occupancy datasets, where head classes (e.g., roads and vegetation) may outnumber tail classes (e.g., bicycles and motorcycles) by several orders of magnitude. This severe class imbalance leads to biased predictions, as models tend to overfit to frequent classes while underperforming on rare ones. While the long-tail problem has been extensively studied in image classification [24, 25, 26], it remains largely unaddressed in the context of 3D occupancy prediction. Furthermore, voxels exhibit inherent geometric distribution patterns. In 3D scenes, objects of the same type often occupy a large continuous space. For example, a road is usually a whole flat area. However, even when facing the same area, the existing method needs to check whether each voxel belongs to the same category. This repetitive work wastes time and computing power, and may even lead to wrong predictions.

In this paper, we propose a new framework SHTOCC, which explores the inter-class distribution and geometric distribution of 3D voxels for the first time, and uses this as prior knowledge to guide the generation of voxels.

Sparse Head-Tail-Voxel Construction. First, to avoid redundant recomputation of homogenized voxels, we propose a novel sparse sampling strategy to construct a very sparse voxel distribution that can correctly describe the geometric distribution of the spatial scene. Specifically, SHTOCC adopts a two-stage selection: (1) attention-guided top-k head voxel extraction to capture the key areas that the model itself pays most attention to; (2) balanced tail voxel sampling using class-specific confidence to extract tail class voxels ignored by the model. This dual mechanism explicitly retains the class information of the head and tail while maintaining computational efficiency.

Decouple Decoder. To address the long-tail problem caused by the imbalanced inter-class distribution, we introduced decoupled learning into 3D Occ named decouple decoder, which separates learning into two distinct phases: (1) Representation learning: the model is trained to learn a general feature representation without class distribution bias; (2) Class-balanced head refinement: Freeze the learned representations and exclusively retrain the segmentation head with label smoothing, strategically redistricting prediction confidence to prevent overfitting on head classes.

Through extensive experiments on the various task including Lidar Segmentation in nuScenes [3], 3D Occupancy prediction in nuScenes-Occupancy [2] and Occ3D-nuScenes [27], Semantic Scene Completion SemanticKITTI [1] benchmarks, we verify that the proposed SHTOCC is an effective solution which can reduce memory overhead, improve inference speed, achieves the real time result and obtain accurate 3D Occ results. Figure 1a and Figure 1b demonstrate that SHTOCC reduces inference time, saves computational memory, and improves prediction accuracy. Figure 1c

demonstrates that the voxels of SHTOcc is much more sparse than SparseOcc [22]. The contributions are summarized as follows:

- We propose a sparse head-tail voxel construction to carefully design sparse voxels, which can accurately extract key voxels while avoiding the model’s excessive focus on head voxels and alleviating the long-tail effect.
- We introduce decoupled training with label smoothing into 3D Occ, which can further prevent the model from focusing too much on the head voxels and improve the prediction accuracy.
- Our method has been embedded in several popular backbone networks, and extensive experiments on various datasets show that our method significantly reduces the memory overhead while improving performance, achieving state-of-the-art performance.

2 Related Work

2.1 3D Occupancy Prediction

Distribution-independent methods. The field of 3D semantic occupancy prediction has evolved significantly since its inception [28, 29, 30]. Early approaches primarily utilized volumetric TSDF representations processed through 3D convolutions [31, 32], while subsequent hybrid methods [33, 34, 35] focused on projecting 2D features into 3D space. Recent camera-based methods have introduced several innovations: MonoScene [36] pioneered purely visual solutions with 3D UNets, TPVFormer [14] developed tri-perspective view representations, and VoxFormer [37] introduced diffusion-based strategies. Other notable advances include mask-wise prediction in OccFormer [6], geometric enhancements in OccDepth [38] and NDCScene [39], and unified scene modeling in OccNet [40]. While these methods demonstrate progressive improvements, they fundamentally treat all voxels equally, ignoring two critical distribution patterns: (1) the inherent sparsity of 3D scenes where most voxels are empty, and (2) the non-uniform semantic distribution across different object categories.

Biased Distribution-Aware Methods. Recent methods exploit voxel sparsity by focusing computation on occupied regions. (1) BEV-based methods [4, 7, 10] compress dense voxels into BEV views, saving space but losing height information. (2) Sparse representation methods, such as TPV [14, 15] use three views to replace dense voxels, SparseOcc [22] prune empty voxels and only keep non-empty voxels, and ProtoOcc [23] use low-resolution queries to replace high-resolution queries. However, existing methods fail to fully utilize the inter-class semantic distribution and geometric regularity in the voxel space, resulting in poor performance. This paper explores and solves the related problems caused by the inter-class distribution and geometric distribution, further improving the prediction accuracy.

2.2 Long Tail Distribution

The long-tail recognition (LTR) problem has been extensively studied in various 2D computer vision tasks, including image classification [24], object detection [25], and semantic segmentation. Popular solutions typically involve class re-weighting [24], re-sampling strategies [25], or the decoupled training paradigm [26]. Recent works like LTWB [24] and LOS [41] have further advanced the field by analyzing the separate effects of representation learning and classifier retraining.

However, Traditional 2D task methods cannot be directly applied to 3D tasks, because 3D data has higher dimensional complexity (such as voxel sparsity and geometric structure sensitivity), simply resampling the tail class voxels will cause the geometric relationship of the 3D scene to be disordered. While long-tail problems have been addressed in many vision domains, no prior work has specifically targeted this issue in 3D occupancy prediction. This paper bridges this gap by adapting decoupled training and label smoothing techniques to 3D Occ, marking the first dedicated effort to solve the long-tail distribution problem in this domain.

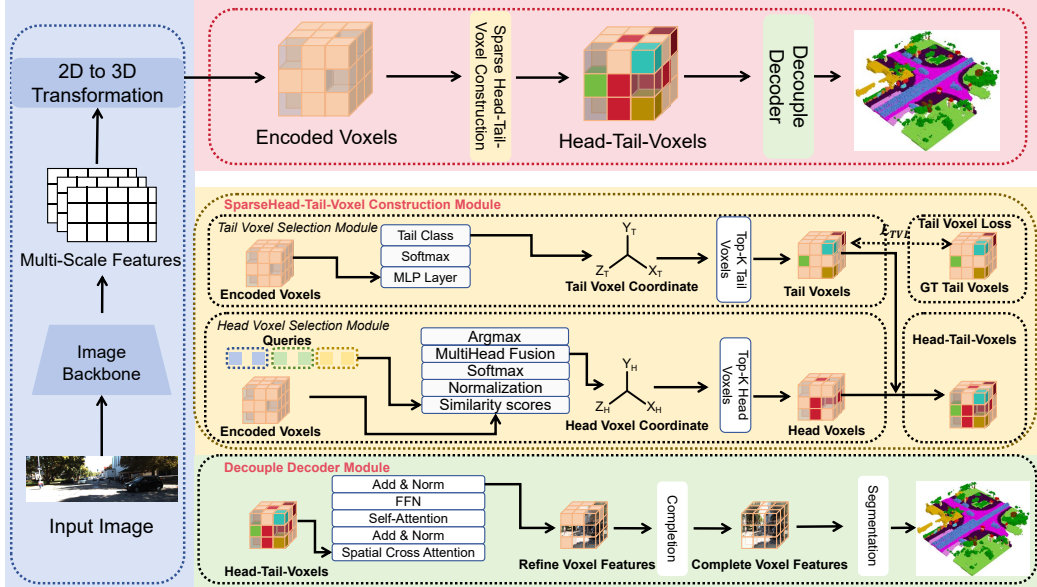


Figure 2: Overview of SHTOcc. The images featured are initially extracted by the image backbone and then convert to 3D encoded voxels through 2D to 3D transformation. The encoded voxel is extracted through dual path to obtain sparse Head and Tail voxels. The entire extraction process is a coarse-to-fine process. With each additional layer, more voxels will be extracted accordingly. In the second learning phase of decouple training, only the parameters of segmentation head will be updated.

3 Methods

3.1 Preliminary

3D Occupancy Prediction. Given a monocular image or a set of images taken by surrounding cameras $I = I_i^N$, the goal of vision-based 3D semantic occupancy prediction is to estimate the state of 3D voxels within the visual range and obtain the dense semantic voxel predictions $V \in \mathbb{R}^{C \times H \times W \times D}$, i.e., to predict the semantic label of each voxel in a predefined 3D voxels based on the known camera intrinsic parameters K_i and extrinsic parameters $[R_i | t_i]$, where N indicates the number of view cameras, C is the number of classes and H, W, D represents the voxel spatial resolutions.

Sparse Representation. According to the observation from SparseOcc [22, 21], about 90% of the voxels in V are empty. Updating the entire voxel requires a lot of time and memory overhead. Therefore, sparse voxel representation is proposed to replace the dense voxel representation to avoid the waste of computing resources. Specifically, dense feature V are converted to a sparse representation by gathering non-empty voxels and the sparse tensor is stored in a commonly used coordinate (COO) format:

$$\mathbb{V} = \{(\mathbf{p}_i = [x_i, y_i, z_i] \in \mathbb{R}^3, \mathbf{f}_i \in \mathbb{R}^C) | i = 1, 2, \dots, N\}. \quad (1)$$

In the above equation, N represents the number of nonempty voxels, while p_i and f_i denote the coordinates and features of the i -th voxel, respectively, all subsequent operations are performed on this sparse representation.

3.2 Method Overview

As shown in Figure 2, we process monocular or multi-view images $I = I_i^N$ through three key stages: First, the multi-scale features $F = F_i^N$ are extracted by 2D image backbone. Then the encoded voxels are obtained through the 2D to 3D transformation module according to the multi-scale features and initial voxel queries. Second, The encoded voxels are passed through the Sparse Head-Tail-Voxel

Construction module to leave the most important sparse head and tail voxels, and these head and tail voxels interact through the 3D backbone to get the preliminary prediction results. Finally, all parameters except the segmentation head are frozen, and decouple learning is performed to get the final output 3D semantic voxels.

3.3 Sparse Head-Tail-Voxel Construction

Head Voxel Selection. In the 3D voxel decoder, a key insight is that only a few important voxels actually need to be updated - but crucially, these important voxels should be determined by the model itself, not by manual observation. This motivates us to use the attention mechanism to automatically identify and prioritize the most task-relevant voxels. The attention mechanism dynamically computes the relevance score between the learned query (Q) and the voxel-based key (K), generating an attention matrix of shape $L \times S$ where each element represents the normalized importance weight (0–1) between the query and the voxel location. Through this process, the model is able to intrinsically learn which voxels are most important for occupancy prediction, as evidenced by their attention weights, eliminating the need to manually set importance criteria, such as non-empty voxels.

As shown in the yellow box in Figure 2, in 3D occupancy prediction tasks, voxel embeddings typically act as keys, while queries are strategically designed according to specific methods. We first measures query-key similarity through dot products $Q \cdot K^T$, producing raw attention scores that quantify spatial relationships across the 3D voxels. These scores then undergo normalization by scaling with $\frac{1}{\sqrt{d_k}}$ to maintain stable gradients in the high-dimensional feature space, where d_k is the feature dimension, followed by row-wise softmax to convert them into probabilistic attention weights that sum to 1 per query, ensuring focused attention on relevant regions. After that, the normalized attention from multiple parallel heads are aggregated through averaging to obtain the attention matrix $M_{atten} \in \mathbb{R}^{L \times S}$, where L denotes the length of queries and S is the length of keys. The attention matrix M_{atten} quantifies the attention weights between all query-key pairs. By taking the argmax along the 0th dimension of M_{atten} , we identify the head voxel coordinates. Specifically, for each key voxel, we determine the query position that assigns it the highest attention weight. This operation effectively extracts the most relevant query for each spatial location in the 3D voxels. Finally, we select top-k voxel coordinates as head voxel coordinates.

Tail Voxel Selection. To address this long-tail distribution problem, SHTOcc adopts a tail voxel selection module, as shown in the yellow box in Figure 2: First, it generates coarse voxel predictions, and then extracts tail voxels equal to the number of head voxels. When the available tail voxels are less than the threshold K , the method applies repetition to enhance its representation. Specifically, given the voxel feature F^{voxel} , the system first generates a coarse prediction P^{coarse} through a single-layer multi-layer perceptron (MLP) with a softmax activation function, formulating the task as a point-by-point segmentation problem:

$$\mathbb{P}^{Tail} = \text{MLP}(F^{Tail}), \quad (2)$$

we define the coordinate of a 3D voxel as a tail voxel coordinate here. Then, for each voxel $P_{i,j,k}^{Tail}$ at the coordinate (i, j, k) , we sort them in descending order according to their tail class probability. Since it is a rough prediction, the tail probability of each voxel may not be accurate, we implement a robust top-K selection strategy. In addition to extracting the voxel with the highest probability of the tail class, we also extract the voxel with the second highest probability of the tail class to ensure that the tail class voxels are robustly extracted without omission. The entire selection process follows the following steps: (1) Extract the voxel $top - 1$ with the highest tail probability. (2) If the number is still less than K , include the voxel $top - 2$ with the second highest probability. (3) Repeat the extraction of these voxels as needed until K samples are reached.

Tail Voxel Loss. In order to further solve the long tail problem, it is not enough to simply extract the tail voxel. It is necessary to use the corresponding tail ground truth in the target to strongly supervise the extracted tail voxel, forcing the model to pay more attention to the tail voxel. SHTOcc uses a method similar to HASSC [42] to calculate its tail voxel loss. First, SHTOcc extracting N tail voxels based on their coarse prediction probabilities $P^{Tail} \in \mathbb{R}^{C_1 \times H \times W \times D}$ and corresponding coordinates $V^{Tail} \in \mathbb{R}^{N \times 3}$, where C_1 represents the number of class and $H \times W \times D$ indicates the spatial shape of voxels. The coordinate V^{Tail} is then used to resample the corresponding features from the fine-grained voxel feature $F^{Tail} \in \mathbb{R}^{C_2 \times H \times W \times D}$ and ground truth $G^{Tail} \in \mathbb{R}^{H \times W \times D}$, where C_2

is the number of channels. The refinement module then processes the concatenated features and predictions through a lightweight MLP to generate refined predictions $P_{Refine}^{Tail} \in \mathbb{R}^{N \times C_1}$. The tail voxel loss is calculated as follows:

$$\mathcal{L}_{TVL} = \text{CE}(P_{Refine}^{Tail}, G^{Tail}), \quad (3)$$

where CE denotes the cross-entropy loss and \mathcal{L}_{TVL} represents the tail voxel loss. Therefore, the total loss of SHTOcc is :

$$\mathcal{L}_{total} = \mathcal{L}_{baseline} + \mathcal{L}_{TVL}, \quad (4)$$

where $\mathcal{L}_{baseline}$ denotes the origin loss of the base line. Adding tail voxel loss can make the model pay more attention to the tail class, thereby improving the overall prediction accuracy

3.4 Decouple Decoder

The most effective way to solve the long-tail problem is to combine decouple learning with data resampling. While this approach works well in 2D tasks, 3D occupancy prediction faces unique challenges: each voxel represents an independent classification task, and resampling the tail class data destroys the geometric structure. Our proposed Sparse Head-Tail-Voxel Construction maintains an equal number of voxels for the head and tail classes while preserving spatial relationships, effectively establishing a voxel resampling framework specifically for 3D spatial reasoning tasks. In addition, our proposed Decouple Decoder enhances decouple learning through label smoothing during classifier optimization, thereby reducing overconfidence in the head class while improving the prediction accuracy of the tail class.

Specifically, our framework implements an iterative refinement process for the selected Head-Tail Voxels. SHTOcc is designed as a plug-and-play module with broad compatibility across different architectures. The refinement pipeline operates as follows: The identified Head-Tail Voxels are first processed through standard 3D decoder components (cross-attention, self-attention, and feed-forward networks, illustrated in Figure 2) to generate refined voxel features. Then, these refined voxel features are then integrated with the encoded voxels through voxel completion. The complete voxel features are finally processed by a segmentation head to produce the semantic voxel predictions. This modular design maintains architectural flexibility while ensuring comprehensive feature refinement through established attention mechanisms and neural network components. Furthermore, we enhance the decoupled learning process through strategic label smoothing during the classifier optimization phase. This modification counteracts model overconfidence in head-class predictions while improving tail-class prediction accuracy, which is shown as following:

$$\mathcal{L}_{LS} = - \sum_{i=1}^N \sum_{c=1}^C \tilde{y}_{i,c} \log(p_{i,c}), \quad \tilde{y}_{i,c} = \begin{cases} 1 - \epsilon_c & \text{if } c = y_i \\ \epsilon_c / (C - 1) & \text{otherwise} \end{cases} \quad (5)$$

where ϵ_c is the smooth factor, C is the number of classes. Our experiments show that adding a small smoothing factor can better balance the category representation while improving the performance of the tail classes.

4 Experiments

4.1 Experiment Setup

Datasets. We evaluate SHTOcc on multiple tasks across three benchmark datasets: SemanticKITTI [1] for semantic scene completion, nuScenes-Occupancy [2] and Occ3D-nuScenes [27] for 3D occupancy prediction, and nuScenes [3] for LiDAR segmentation. **SemanticKITTI** provides 22 sequences with monocular images, LiDAR point clouds, segmentation labels, and semantic scene completion annotations, using sequences 00-10 (excluding 08) for training, sequence 08 for validation, and sequences 11-21 for testing, with each voxel labeled as either empty or one of 19 semantic classes. **NuScenes-Occupancy** extends nuScenes with dense 3D semantic occupancy annotations (1 empty class and 16 semantic classes) through an Augmenting and Purifying pipeline, covering 700 training and 150 validation scenes while utilizing the original nuScenes' multi-view images and LiDAR points. **Occ3D-nuScenes** is a large-scale autonomous driving dataset containing 700 training and

150 validation scenes with 17 semantic categories (16 object classes plus "empty"). The **nuScenes** dataset contains 1000 driving sequences (20s each) from Boston and Singapore with 2Hz key-frame 3D bounding box annotations. Following Occformer [6], we train SHTOcc using sparse LiDAR point supervision under the official 700/150/150 train/val/test split for 3D semantic occupancy prediction.

Evaluation Metric. We report the mean intersection over union (mIoU) for both the semantic scene completion (SSC) and the LiDAR segmentation tasks. For computational efficiency, we report inference time, training memory consumption in SemanticKITTI dataset following ProtoOcc [23], we additionally report training memory, 3D/Overall Latency in nuScenes-Occupancy dataset following the settings from SparseOcc [22].

Implementation Details. We integrate SHTOcc into several state-of-the-art semantic scene completion methods on the SemanticKITTI dataset, including SparseOcc [22] and Symphonize [43]. Following ProtoOcc [23], we evaluate Symphonize-SHTOcc in three configurations: original, base, and small, with query sizes of $128 \times 128 \times 8$, $128 \times 128 \times 16$, and $64 \times 64 \times 8$, respectively. Then, we extend our evaluation to 3D occupancy prediction by integrating SHTOcc into SparseOcc [22] on the nuScenes-Occupancy dataset [2] and into COTR [11] on the Occ3D-nuScenes dataset [27]. Furthermore we integrate SHTOcc to LiDAR segmentation by incorporating it into Occformer [6] on the nuScenes dataset.

4.2 Experimental Results

Semantic Scene Completion. As shown in Table 1, we report the quantitative comparison of existing state-of-the-art methods for semantic scene completion tasks on SemanticKITTI datasets, the results are evaluated on the test set. In comparison with the lightweight method SparseOcc, SHTOcc can be further lightweight and improve the performance. What's more, under the query settings of different resolutions proposed by ProtoOCC, the mIoU of SHTOcc is significantly better than symphonize and ProtoOcc, with an improvement of about 0.3 compared to ProtoOcc and about 0.7 compared to symphonize. For efficiency evaluation, We can observe that SHTOcc can improve the inference speed and save training memory by comparing to all baselines. Specifically, SHTOcc reduces the inference time by up to 58.6% when compared with ProtoOcc-s, and saves up to 42.2% of training memory when compared with symphonize-o. These results show the superiority of SHTOcc in saving computational overhead.

Table 1: **Quantitative results on SemanticKITTI test.** * denotes the results provided by its official paper.

Method	mIoU	Inf.	Time	Memory	Semantic Categories																
					road (15.9%)	sidewalk (11.8%)	parking (1.12%)	other-grnd. (0.56%)	building (14.1%)	car (3.02%)	truck (0.16%)	bicycle (0.05%)	motorcycle (0.05%)	other-veh. (0.05%)	vegetation (3.95%)	trunk (0.15%)	terrain (91.7%)	person (0.07%)	bicyclist (0.05%)	motorcyclist (0.05%)	fence (3.0%)
LMSCNet* [44]	7.07	-	-	46.70 19.50 13.50 3.10 10.30 14.30 0.30 0.00 0.00 0.00 10.80 0.00 10.40 0.00 0.00 0.00 5.40 0.00 0.00																	
AICNet* [34]	7.09	-	-	39.30 18.30 19.80 1.60 9.60 15.30 0.70 0.00 0.00 0.00 9.60 1.90 13.50 0.00 0.00 0.00 5.00 0.10 0.00																	
JS3C-Net* [45]	8.97	-	-	47.30 21.70 19.90 2.80 12.70 20.10 0.80 0.00 0.00 0.00 4.10 14.20 3.10 12.40 0.00 0.20 0.20 8.70 1.90 0.30																	
MonoScene* [36]	11.08	-	-	54.70 27.10 24.80 5.70 14.40 18.80 3.30 0.50 0.70 4.40 14.90 2.40 19.50 1.00 1.40 0.40 11.10 3.30 2.10																	
TPVFormer* [14]	11.26	-	-	55.10 27.20 27.40 6.50 14.80 19.20 3.70 1.00 0.50 2.30 13.90 2.60 20.40 1.10 2.40 0.30 11.00 2.90 1.50																	
OccFormer* [6]	12.32	-	-	55.90 30.30 31.50 6.50 15.70 21.60 1.20 1.50 1.70 3.20 16.80 3.90 21.30 2.20 1.10 0.20 11.90 3.80 3.70																	
HASSC* [42]	13.34	-	-	54.60 27.70 23.80 6.20 21.10 28.40 4.70 1.60 1.00 3.90 23.80 8.50 23.30 1.60 4.00 0.30 13.01 5.80 5.50																	
VoxFormer* [37]	12.20	-	-	53.90 25.30 21.10 5.60 19.80 20.80 3.50 1.00 0.70 3.70 22.40 7.50 21.30 1.40 2.60 0.20 11.10 5.10 4.90																	
SparseOcc* [22]	11.83	51.68ms	13361M	55.80 28.40 31.70 5.10 16.00 21.70 0.00 1.60 0.70 3.40 16.40 4.10 21.30 0.00 0.00 0.00 11.70 3.90 3.00																	
Ours (+SparseOcc)	12.11	50.19ms	11819M	53.90 28.60 27.70 7.10 16.10 21.80 2.00 1.00 1.60 8.80 16.20 4.10 21.00 1.20 0.40 0.00 11.70 3.70 3.20																	
Symphonies-o* [43]	15.04	39.79ms	18000M	58.40 29.30 26.90 11.70 24.70 23.60 3.20 3.60 2.60 5.60 24.20 10.00 23.10 3.20 1.90 2.00 16.10 7.70 8.00																	
Ours (+Symphonies-o)	15.13	25.38ms	10400M	57.80 28.90 26.30 12.00 23.40 24.60 3.60 3.50 1.80 4.60 24.90 11.00 22.50 3.70 3.80 0.10 17.10 8.70 9.40																	
ProtoOcc-S* [23]	14.36	40.80ms	-	57.20 30.40 30.00 10.10 24.50 23.20 2.80 2.00 1.70 4.30 24.50 8.10 23.20 2.30 2.20 0.40 14.60 6.20 6.30																	
Symphonies-S* [43]	14.07	23.50ms	14000M	57.60 29.40 29.00 10.50 24.20 22.00 2.70 2.00 1.80 4.70 23.80 7.50 22.80 2.10 1.40 0.70 13.80 5.60 5.70																	
Ours (+Symphonies-S)	14.74	16.91ms	8110M	57.40 29.20 26.20 11.60 23.20 22.70 2.10 4.10 2.20 6.60 23.90 9.00 23.70 4.20 3.50 0.50 15.30 7.30 7.50																	
ProtoOcc-B* [23]	14.77	76.20ms	-	57.90 28.60 27.60 10.20 24.30 24.10 3.10 3.30 3.20 4.70 25.00 9.20 22.60 3.40 2.00 1.50 15.60 7.30 6.90																	
Symphonies-B* [43]	14.50	49.10ms	24100M	57.00 28.00 27.50 9.10 24.10 23.70 3.70 3.60 2.40 4.40 24.60 9.90 22.50 2.90 1.70 0.50 15.70 7.50 7.00																	
Ours (+Symphonies-B)	15.07	38.75ms	15000M	58.30 29.00 26.30 10.80 22.50 24.40 4.30 2.30 4.00 25.30 10.60 22.90 3.80 2.40 0.30 17.10 8.50 9.10																	

3D Occupancy Prediction. We integrate SHTOcc into SparseOcc [22] on the nuScenes-Occupancy dataset [2] in Table 2 and integrate SHTOcc into COTR [11] on the Occ3D-nuScenes dataset [27] in Table 3 to evaluate 3D occupancy prediction. The mIoU is improved by 0.7 points and 0.2 points on sparseOcc and COTR respectively. In particular, the training memory and inference time of SHTOcc are improved by 7% and 25% respectively compared to SparseOcc. It should be emphasized that SparseOcc itself is a lightweight method, SHTOcc is even lighter and mIoU can be improved.

Table 2: **Semantic occupancy prediction results on nuScenes-Occupancy [2] validation set.** * represents the results provided by [22]. †denotes the reproduced results by its official code.

Method	Input	mIoU	Memory	3D/Overall Latency	Category															
					barrier	bicycle	bus	car	const. veh.	motorcycle	pedestrian	traffic cone	trailer	truck	drive. suf.	other flat	sidewalk	terrain	mammal	vegetation
MonoScene* [36]	C	6.9	-	-	7.1	3.9	9.3	7.2	5.6	3.0	5.9	4.4	4.9	4.2	14.9	6.3	7.9	7.4	10.0	7.6
TPVFormer* [14]	C	7.8	20G	0.57/0.73s	9.3	4.1	11.3	10.1	5.2	4.3	5.9	5.3	6.8	6.5	13.6	9.0	8.3	8.0	9.2	8.2
OpenOccupancy* [2]	C	10.3	19G	0.84/1.22s	9.9	6.8	11.2	11.5	6.3	8.4	8.6	4.3	4.2	9.9	22.0	15.8	14.1	13.5	7.3	10.2
C-CONet* [2]	C	12.8	21G	2.18/2.58s	13.2	8.1	15.4	17.2	6.3	11.2	10.0	8.3	4.7	12.1	31.4	18.8	18.7	16.3	4.8	8.2
SparseOcc † [22]	C	13.1	15G	0.06/0.12s	15.7	7.3	15.3	17.6	6.1	8.1	10.6	9.4	5.5	12.9	30.8	21.7	19.1	16.1	4.9	8.6
Ours (+SparseOcc)	C	13.8	14G	0.04/0.09s	15.9	8.6	14.9	18.3	7.3	9.4	10.8	9.1	6.5	13.2	31.0	21.3	20.3	18.4	6.1	10.4

Table 3: Semantic occupancy prediction results on Occ3D-nuScenes [27] validation set. * represents the results provided by its official paper.

Method	Venue	Image Backbone	Epoch	Visible Mask	mIoU (%)
MonoScene* [36]	CVPR'22	ResNet-101	24	✗	6.1
OccFormer* [6]	ICCV'23	ResNet-50	24	✗	20.4
BEVFormer* [46]	ECCV'22	ResNet-101	24	✗	26.9
CTF-Occ* [27]	arXiv'23	ResNet-101	24	✗	28.5
VoxFormer* [37]	CVPR'23	ResNet-101	24	✓	40.7
SurroundOcc* [5]	ICCV'23	InternImage-B	24	✓	40.7
FBOcc* [47]	ICCV'23	ResNet-50	20	✓	42.1
PanoOcc* [48]	CVPR'24	-	24	✓	38.1
ProtoOcc-CVPR* [23]	CVPR'25	-	24	✓	39.0
ProtoOcc-AAAI* [49]	AAAI'25	ResNet-50	24	✓	39.6
STCOcc* [13]	CVPR'25	ResNet-50	24	✓	44.6
COTR+BEVDet3D* [11]	CVPR'24	ResNet-50	24	✓	44.5
Ours (+COTR)	-	ResNet-50	24	✓	44.7

LiDAR Segmentation. We assign the voxel predictions on sparse LiDAR points for the semantic segmentation evaluation. As shown in Table 4, we report the quantitative comparison of existing state-of-the-art methods for LiDAR segmentation tasks on nuScenes validation set followed [48]. In this setting, SHTOcc is integrated into Occformer and implement the R101-DCN as image backbone. The result shows that with SHTOcc, the mIOU of occformer improves 0.6%. Additionally, the tail class such as construction vehicle and motorcycle improves significantly, shows the improvement of SHTOcc in task of LiDAR Segmentation.

Visualization. Figure 3 demonstrates the visualization results of SparseOcc [22] and SHTOcc. SparseOcc selects all non-empty voxels when constructing sparse voxels, but this selection strategy will be affected by many uncritical voxels, resulting in incorrect prediction results. In contrast, SHTOcc uses the most important voxels that the model focuses on, and the number of selected voxels is much smaller than SparseOcc, but it can make more accurate predictions. As shown in Figure 3a and Figure 3b, motorcycles and roads are predicted as people and trucks, while SHTOcc predicts correctly.

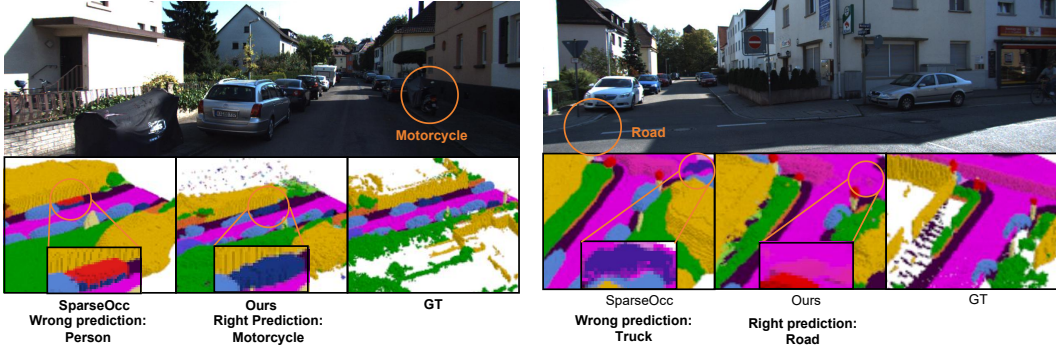
5 Ablation Study

In this section we evaluate the effectiveness of different components and different tail class groups, more ablation study will be shown in supplementary materials.

Ablation on different components. In order to gain a deeper understanding of the functions of each part, we evaluated the performance improvement of each module in Table 5. After using the head voxel selection module instead of dense prediction, along with the reduction in computational overhead, the performance also decreased slightly, and mIOU dropped by about 0.5 points. After adding the tail voxel selection module, mIOU increased a little bit, indicating that the tail class voxel is indeed ignored by the model. Adding this part helps the model focus on the voxels of the tail class. After adding Tail voxel loss, mIOU increased by about 0.2 points, indicating that tail voxel loss is also helpful in guiding the model to pay attention to the tail class voxels. After adding decouple learning,

Table 4: LiDAR semantic segmentation results on nuScenes validation set. * denotes the results provided by the official paper.

Method	Input Modality	Image Backbone	mIoU	barrier	bicycle	bus	car	const. veh.	motorcycle	pedestrian	traffic cone	trailer	truck	drive. surf.	other flat	sidewalk	terrain	manmade	vegetation
				orange	pink	yellow	blue	cyan	yellow	pink	yellow	blue	yellow	yellow	grey	purple	green	green	
RangeNet++* [50]	LiDAR	-	65.5	66.0	21.3	77.2	80.9	30.2	66.8	69.6	52.1	54.2	72.3	94.1	66.6	63.5	70.1	83.1	79.8
PolarNet* [51]	LiDAR	-	71.0	74.7	28.2	85.3	90.9	35.1	77.5	71.3	58.8	57.4	76.1	96.5	71.1	74.7	74.0	87.3	85.7
Salsanext* [52]	LiDAR	-	72.2	74.8	34.1	85.9	88.4	42.2	72.4	72.2	63.1	61.3	76.5	96.0	70.8	71.2	71.5	86.7	84.4
Cylinder3D++* [53]	LiDAR	-	76.1	76.4	40.3	91.2	93.8	51.3	78.0	78.9	64.9	62.1	84.4	96.8	71.6	76.4	75.4	90.5	87.4
RPVNet [54]	LiDAR	-	77.6	78.2	43.4	92.7	93.2	49.0	85.7	80.5	66.0	66.9	84.0	96.9	73.5	75.9	76.0	90.6	88.9
BEVFormer-Base* [46]	Camera	R101-DCN	56.2	54.0	22.8	76.7	74.0	45.8	53.1	44.5	24.7	54.7	65.5	88.5	58.1	50.5	52.8	71.0	63.0
TPVFormer-Base* [14]	Camera	R101-DCN	68.9	70.0	40.9	93.7	85.6	49.8	68.4	59.7	38.2	65.3	83.0	93.3	64.4	64.3	64.5	81.6	79.3
Occformer* [6]	Camera	R101-DCN	70.4	70.3	43.8	93.2	85.2	52.0	59.1	67.6	45.4	64.4	84.5	93.8	68.2	67.8	68.3	82.1	80.4
Ours (+Occformer)	Camera	R101-DCN	71.0	70.3	43.2	92.0	84.3	56.0	73.5	64.8	43.1	65.0	85.0	93.4	66.5	68.0	68.5	81.8	80.1



(a) Visualization (a). SparseOcc [22] predicts motorcycle as person, while SHTOCC predicts it correctly. (b) Visualization (b). SparseOcc [22] predicts road as truck, while SHTOCC predicts it correctly.

Figure 3: Visualization of SparseOcc [22] and SHTOCC. The figure demonstrates that SHTOCC can achieve more accurate predictions with lower computation cost.

mIoU continued to increase by 0.3 points, which also highlights the contribution of decouple learning to the long-tail distribution problem.

Table 5: Ablation study on different modules.

Baseline.	Head Voxel Selec.	Tail Voxel Selec.	Tail Voxel Loss.	Decouple Learning	Memory	mIoU
✓					18000M	14.59
✓	✓				10400M	14.05
✓	✓	✓			10400M	14.18
✓	✓	✓	✓		10400M	14.40
✓	✓	✓	✓	✓	4870M	14.75

6 Conclusion

In this paper, we introduce SHTOCC, a plug-and-play method for saving computational overhead without losing performance. SHTOCC extracts key voxels and updates them based on the attention mechanism and the distribution of the tail class voxels, and introduces decouple learning to eliminate the influence of the long-tail distribution. Extensive experiments show that SHTOCC can improve prediction accuracy while saving computational overhead. We expect SHTOCC to inspire future research and contribute to the progress of autonomous driving and 3D perception.

References

- [1] J. Behley, M. Garbade, A. Milioto, J. Quenzel, S. Behnke, C. Stachniss, and J. Gall, “Semantickitti: A dataset for semantic scene understanding of lidar sequences,” in *Proceedings of the IEEE/CVF international conference on computer vision*, 2019, pp. 9297–9307.
- [2] X. Wang, Z. Zhu, W. Xu, Y. Zhang, Y. Wei, X. Chi, Y. Ye, D. Du, J. Lu, and X. Wang, “Openoccupancy: A large scale benchmark for surrounding semantic occupancy perception,” in *Proceedings of the IEEE/CVF International Conference on Computer Vision*, 2023, pp. 17 850–17 859.
- [3] H. Caesar, V. Bankiti, A. H. Lang, S. Vora, V. E. Liong, Q. Xu, A. Krishnan, Y. Pan, G. Baldan, and O. Beijbom, “nuscenes: A multimodal dataset for autonomous driving,” in *Proceedings of the IEEE/CVF conference on computer vision and pattern recognition*, 2020, pp. 11 621–11 631.
- [4] Z. Ming, J. S. Berrio, M. Shan, and S. Worrall, “Inversematrixvt3d: An efficient projection matrix-based approach for 3d occupancy prediction,” in *2024 IEEE/RSJ International Conference on Intelligent Robots and Systems (IROS)*. IEEE, 2024, pp. 9565–9572.
- [5] Y. Wei, L. Zhao, W. Zheng, Z. Zhu, J. Zhou, and J. Lu, “Surroundocc: Multi-camera 3d occupancy prediction for autonomous driving,” in *Proceedings of the IEEE/CVF International Conference on Computer Vision*, 2023, pp. 21 729–21 740.
- [6] Y. Zhang, Z. Zhu, and D. Du, “Occformer: Dual-path transformer for vision-based 3d semantic occupancy prediction,” in *Proceedings of the IEEE/CVF International Conference on Computer Vision*, 2023, pp. 9433–9443.
- [7] J. Hou, X. Li, W. Guan, G. Zhang, D. Feng, Y. Du, X. Xue, and J. Pu, “Fastocc: Accelerating 3d occupancy prediction by fusing the 2d bird’s-eye view and perspective view,” in *2024 IEEE International Conference on Robotics and Automation (ICRA)*. IEEE, 2024, pp. 16 425–16 431.
- [8] M. Lu, Y. Huang, J. Liu, X. Huang, D. Li, J. Peng, L. Tian, and E. Barsoum, “Fast occupancy network,” *arXiv preprint arXiv:2412.07163*, 2024.
- [9] Y. Tian, S. Bai, Z. Luo, Y. Wang, Y. Lv, and F.-Y. Wang, “Mambocc: Visual state space model for bev-based occupancy prediction with local adaptive reordering,” *arXiv preprint arXiv:2408.11464*, 2024.
- [10] Z. Yu, C. Shu, J. Deng, K. Lu, Z. Liu, J. Yu, D. Yang, H. Li, and Y. Chen, “Flashocc: Fast and memory-efficient occupancy prediction via channel-to-height plugin,” *arXiv preprint arXiv:2311.12058*, 2023.
- [11] Q. Ma, X. Tan, Y. Qu, L. Ma, Z. Zhang, and Y. Xie, “Cotr: Compact occupancy transformer for vision-based 3d occupancy prediction,” in *Proceedings of the IEEE/CVF Conference on Computer Vision and Pattern Recognition*, 2024, pp. 19 936–19 945.
- [12] D. Chen, H. Zheng, J. Fang, X. Dong, X. Li, W. Liao, T. He, P. Peng, and J. Shen, “Rethinking temporal fusion with a unified gradient descent view for 3d semantic occupancy prediction,” *arXiv preprint arXiv:2504.12959*, 2025.
- [13] Z. Liao, P. Wei, S. Chen, H. Wang, and Z. Ren, “Stcocc: Sparse spatial-temporal cascade renovation for 3d occupancy and scene flow prediction,” *arXiv preprint arXiv:2504.19749*, 2025.
- [14] Y. Huang, W. Zheng, Y. Zhang, J. Zhou, and J. Lu, “Tri-perspective view for vision-based 3d semantic occupancy prediction,” in *Proceedings of the IEEE/CVF conference on computer vision and pattern recognition*, 2023, pp. 9223–9232.
- [15] J. Zhang, Y. Zhang, Q. Liu, and Y. Wang, “Lightweight spatial embedding for vision-based 3d occupancy prediction,” *arXiv preprint arXiv:2412.05976*, 2024.
- [16] J. Liang, H. Yin, X. Qi, J. J. Park, M. Sun, R. Madhivanan, and D. Manocha, “Et-former: Efficient triplane deformable attention for 3d semantic scene completion from monocular camera,” *arXiv preprint arXiv:2410.11019*, 2024.
- [17] Y. Huang, W. Zheng, Y. Zhang, J. Zhou, and J. Lu, “Gaussianformer: Scene as gaussians for vision-based 3d semantic occupancy prediction,” in *European Conference on Computer Vision*. Springer, 2024, pp. 376–393.

- [18] H. Jiang, L. Liu, T. Cheng, X. Wang, T. Lin, Z. Su, W. Liu, and X. Wang, “Gausstr: Foundation model-aligned gaussian transformer for self-supervised 3d spatial understanding,” *arXiv preprint arXiv:2412.13193*, 2024.
- [19] Y. Huang, A. Thammatadatrakoon, W. Zheng, Y. Zhang, D. Du, and J. Lu, “Probabilistic gaussian superposition for efficient 3d occupancy prediction,” *arXiv preprint arXiv:2412.04384*, 2024.
- [20] J. Wang, Z. Liu, Q. Meng, L. Yan, K. Wang, J. Yang, W. Liu, Q. Hou, and M.-M. Cheng, “Opus: occupancy prediction using a sparse set,” *arXiv preprint arXiv:2409.09350*, 2024.
- [21] H. Liu, Y. Chen, H. Wang, Z. Yang, T. Li, J. Zeng, L. Chen, H. Li, and L. Wang, “Fully sparse 3d occupancy prediction,” in *European Conference on Computer Vision*. Springer, 2024, pp. 54–71.
- [22] P. Tang, Z. Wang, G. Wang, J. Zheng, X. Ren, B. Feng, and C. Ma, “Sparseocc: Rethinking sparse latent representation for vision-based semantic occupancy prediction,” in *Proceedings of the IEEE/CVF Conference on Computer Vision and Pattern Recognition*, 2024, pp. 15 035–15 044.
- [23] G. Oh, S. Kim, H. Ko, H.-g. Chi, J. Kim, D. Lee, D. Ji, S. Choi, S. Jang, and S. Kim, “3d occupancy prediction with low-resolution queries via prototype-aware view transformation,” *arXiv preprint arXiv:2503.15185*, 2025.
- [24] S. Alshammari, Y.-X. Wang, D. Ramanan, and S. Kong, “Long-tailed recognition via weight balancing,” in *Proceedings of the IEEE/CVF conference on computer vision and pattern recognition*, 2022, pp. 6897–6907.
- [25] T. Wang, Y. Li, B. Kang, J. Li, J. Liew, S. Tang, S. Hoi, and J. Feng, “The devil is in classification: A simple framework for long-tail instance segmentation,” in *Computer Vision–ECCV 2020: 16th European Conference, Glasgow, UK, August 23–28, 2020, Proceedings, Part XIV 16*. Springer, 2020, pp. 728–744.
- [26] B. Kang, S. Xie, M. Rohrbach, Z. Yan, A. Gordo, J. Feng, and Y. Kalantidis, “Decoupling representation and classifier for long-tailed recognition,” *arXiv preprint arXiv:1910.09217*, 2019.
- [27] X. Tian, T. Jiang, L. Yun, Y. Mao, H. Yang, Y. Wang, Y. Wang, and H. Zhao, “Occ3d: A large-scale 3d occupancy prediction benchmark for autonomous driving,” *Advances in Neural Information Processing Systems*, vol. 36, pp. 64 318–64 330, 2023.
- [28] L. Mescheder, M. Oechsle, M. Niemeyer, S. Nowozin, and A. Geiger, “Occupancy networks: Learning 3d reconstruction in function space,” in *Proceedings of the IEEE/CVF conference on computer vision and pattern recognition*, 2019, pp. 4460–4470.
- [29] S. Peng, M. Niemeyer, L. Mescheder, M. Pollefeys, and A. Geiger, “Convolutional occupancy networks,” in *Computer Vision–ECCV 2020: 16th European Conference, Glasgow, UK, August 23–28, 2020, Proceedings, Part III 16*. Springer, 2020, pp. 523–540.
- [30] S. Song, F. Yu, A. Zeng, A. X. Chang, M. Savva, and T. Funkhouser, “Semantic scene completion from a single depth image,” in *Proceedings of the IEEE conference on computer vision and pattern recognition*, 2017, pp. 1746–1754.
- [31] J. Li, Y. Liu, D. Gong, Q. Shi, X. Yuan, C. Zhao, and I. Reid, “Rgbd based dimensional decomposition residual network for 3d semantic scene completion,” in *Proceedings of the IEEE/CVF Conference on Computer Vision and Pattern Recognition*, 2019, pp. 7693–7702.
- [32] P. Zhang, W. Liu, Y. Lei, H. Lu, and X. Yang, “Cascaded context pyramid for full-resolution 3d semantic scene completion,” in *Proceedings of the IEEE/CVF International Conference on Computer Vision*, 2019, pp. 7801–7810.
- [33] Y.-X. Guo and X. Tong, “View-volume network for semantic scene completion from a single depth image,” *arXiv preprint arXiv:1806.05361*, 2018.
- [34] J. Li, K. Han, P. Wang, Y. Liu, and X. Yuan, “Anisotropic convolutional networks for 3d semantic scene completion,” in *Proceedings of the IEEE/CVF Conference on Computer Vision and Pattern Recognition*, 2020, pp. 3351–3359.
- [35] S. Liu, Y. Hu, Y. Zeng, Q. Tang, B. Jin, Y. Han, and X. Li, “See and think: Disentangling semantic scene completion,” *Advances in Neural Information Processing Systems*, vol. 31, 2018.

[36] A.-Q. Cao and R. De Charette, “Monoscene: Monocular 3d semantic scene completion,” in *Proceedings of the IEEE/CVF Conference on Computer Vision and Pattern Recognition*, 2022, pp. 3991–4001.

[37] Y. Li, Z. Yu, C. Choy, C. Xiao, J. M. Alvarez, S. Fidler, C. Feng, and A. Anandkumar, “Voxformer: Sparse voxel transformer for camera-based 3d semantic scene completion,” in *Proceedings of the IEEE/CVF conference on computer vision and pattern recognition*, 2023, pp. 9087–9098.

[38] R. Miao, W. Liu, M. Chen, Z. Gong, W. Xu, C. Hu, and S. Zhou, “Occdepth: A depth-aware method for 3d semantic scene completion,” *arXiv preprint arXiv:2302.13540*, 2023.

[39] J. Yao, C. Li, K. Sun, Y. Cai, H. Li, W. Ouyang, and H. Li, “Ndc-scene: Boost monocular 3d semantic scene completion in normalized device coordinates space,” in *2023 IEEE/CVF International Conference on Computer Vision (ICCV)*. IEEE Computer Society, 2023, pp. 9421–9431.

[40] W. Tong, C. Sima, T. Wang, L. Chen, S. Wu, H. Deng, Y. Gu, L. Lu, P. Luo, D. Lin *et al.*, “Scene as occupancy,” in *Proceedings of the IEEE/CVF International Conference on Computer Vision*, 2023, pp. 8406–8415.

[41] S. Sun, H. Lu, J. Li, Y. Xie, T. Li, X. Yang, L. Zhang, and J. Yan, “Rethinking classifier re-training in long-tailed recognition: Label over-smooth can balance,” in *The Thirteenth International Conference on Learning Representations*.

[42] S. Wang, J. Yu, W. Li, W. Liu, X. Liu, J. Chen, and J. Zhu, “Not all voxels are equal: Hardness-aware semantic scene completion with self-distillation,” in *Proceedings of the IEEE/CVF Conference on Computer Vision and Pattern Recognition*, 2024, pp. 14 792–14 801.

[43] H. Jiang, T. Cheng, N. Gao, H. Zhang, T. Lin, W. Liu, and X. Wang, “Symphonize 3d semantic scene completion with contextual instance queries,” in *Proceedings of the IEEE/CVF Conference on Computer Vision and Pattern Recognition*, 2024, pp. 20 258–20 267.

[44] L. Roldao, R. De Charette, and A. Verroust-Blondet, “Lmscnet: Lightweight multiscale 3d semantic completion,” in *2020 International Conference on 3D Vision (3DV)*. IEEE, 2020, pp. 111–119.

[45] X. Yan, J. Gao, J. Li, R. Zhang, Z. Li, R. Huang, and S. Cui, “Sparse single sweep lidar point cloud segmentation via learning contextual shape priors from scene completion,” in *Proceedings of the AAAI conference on artificial intelligence*, vol. 35, no. 4, 2021, pp. 3101–3109.

[46] Z. Li, W. Wang, H. Li, E. Xie, C. Sima, T. Lu, Y. Qiao, and J. Dai, “Bevformer: Learning bird’s-eye-view representation from multi-camera images via spatiotemporal transformers,” *arXiv preprint arXiv:2203.17270*, 2022.

[47] Z. Li, Z. Yu, W. Wang, A. Anandkumar, T. Lu, and J. M. Alvarez, “Fb-bev: Bev representation from forward-backward view transformations,” in *Proceedings of the IEEE/CVF International Conference on Computer Vision*, 2023, pp. 6919–6928.

[48] Y. Wang, Y. Chen, X. Liao, L. Fan, and Z. Zhang, “Panoocc: Unified occupancy representation for camera-based 3d panoptic segmentation,” in *Proceedings of the IEEE/CVF conference on computer vision and pattern recognition*, 2024, pp. 17 158–17 168.

[49] J. Kim, C. Kang, D. Lee, S. Choi, and J. W. Choi, “Protoocc: Accurate, efficient 3d occupancy prediction using dual branch encoder-prototype query decoder,” in *Proceedings of the AAAI Conference on Artificial Intelligence*, vol. 39, no. 4, 2025, pp. 4284–4292.

[50] A. Milioto, I. Vizzo, J. Behley, and C. Stachniss, “Rangenet++: Fast and accurate lidar semantic segmentation,” in *2019 IEEE/RSJ international conference on intelligent robots and systems (IROS)*. IEEE, 2019, pp. 4213–4220.

[51] Y. Zhang, Z. Zhou, P. David, X. Yue, Z. Xi, B. Gong, and H. Foroosh, “Polarnet: An improved grid representation for online lidar point clouds semantic segmentation,” in *Proceedings of the IEEE/CVF conference on computer vision and pattern recognition*, 2020, pp. 9601–9610.

[52] T. Cortinhal, G. Tzelepis, and E. Erdal Aksoy, “Salsanext: Fast, uncertainty-aware semantic segmentation of lidar point clouds,” in *Advances in Visual Computing: 15th International Symposium, ISVC 2020, San Diego, CA, USA, October 5–7, 2020, Proceedings, Part II 15*. Springer, 2020, pp. 207–222.

- [53] X. Zhu, H. Zhou, T. Wang, F. Hong, Y. Ma, W. Li, H. Li, and D. Lin, “Cylindrical and asymmetrical 3d convolution networks for lidar segmentation,” in *Proceedings of the IEEE/CVF conference on computer vision and pattern recognition*, 2021, pp. 9939–9948.
- [54] J. Xu, R. Zhang, J. Dou, Y. Zhu, J. Sun, and S. Pu, “Rpvnet: A deep and efficient range-point-voxel fusion network for lidar point cloud segmentation,” in *Proceedings of the IEEE/CVF international conference on computer vision*, 2021, pp. 16 024–16 033.